



# Influence of patterned surface in the rheometry of simple and complex fluids <sup>☆</sup>



Diana Broboana, Nicoleta Octavia Tanase, Corneliu Balan <sup>\*</sup>

*"Politehnica" University of Bucharest, REOROM Laboratory, Hydraulics Department, Splaiul Independentei 313, 060042 Bucharest, Romania*

## ARTICLE INFO

### Article history:

Received 29 May 2014

Received in revised form 8 October 2014

Accepted 15 October 2014

Available online 24 October 2014

### Keywords:

Rheometry

Patterned surfaces

Microgeometries

Apparent slip

Numerical simulations

## ABSTRACT

The influence of the surface microgeometry in rheometry is investigated using the correlation between experiments and numerical simulations of the flow in plate–plate rotational geometry. The presence of micropillars or microchannels on the plates induces effective or apparent slip of the fluids at the walls generating a “dynamic hydrophobic surface”. The end/edge effects and the gap error are first estimated for the plate–plate smooth geometry, the computational results being found consistent with the performed experiments. The comparison between the measured torques in smooth and microchannels patterned configurations are analyzed using the numerical simulations performed by the Fluent code for the Newtonian fluid and the Carreau model.

The present study demonstrates that hydrophobic effects can be induced at the walls, without the violation of the no-slip condition, by changing the local flow spectrum due to the presence of patterned surfaces at the solid boundary. The results confirm that computational rheometry is an useful tool not just to interpret the experimental data but to calculate the errors of the measurements, as well as to explore and model flow phenomenon as the apparent slip.

The applications of the paper are meant to develop novel testing procedures in rheometry and to design micro-patterned surfaces for the control of slip/adherence of simple and complex liquids in microfluidic devices.

© 2014 Elsevier B.V. All rights reserved.

## 1. Introduction

Microfluidics is today one of the most dynamic domain of study in engineering, especially in relation with novel Lab-on-a-Chip applications which involve the flows of simple and complex fluids [1–3]. One important subject of investigation in microfluidics is the prediction of the fluid behavior in the very vicinity of the walls. Is the fluid slipping or not to the wall? [4,5]; is the surface hydrophilic or hydrophobic in respect to a particular dynamic process? [6–8]; which is the most indicated pattern of the wall to induce hydrophobicity? [9–11], are inevitable questions whose answers would be an important impact in the design procedure of the new devices and applications [12]. Therefore, the control of wall adherence and degree of slipping become central topics for the fundamental studies in microfluidics. If the material surface and the fluid sample are well defined, in order to control the degree of fluid adherence to the walls then we have to design the proper micropattern which induces the desired phenomenon (i.e. total/

partial adherence or slipping). The rheological bulk properties of liquids are experimentally determined using rheometers and special designed measurements procedures based on viscometric flows [13]. In all commercial rheometers (rotational or capillary), the solid surfaces in contact with tested liquids are normally smooth and the slip or perfect adherence of the samples to these surfaces are analyzed and interpreted for each type of measurement, mainly in relation with the microstructure and formulation of the liquid samples [14–17].

The goal of the present study is to investigate and analyze the influence of patterned surfaces in rheometry, to model the flow in plate and plate rotational geometry and to understand how the presence of microgeometries on the plate's surface induces the apparent slipping at the wall and creates “dynamic hydrophobic surfaces”, even if the fluid is considered to adhere to the solid walls.

In 1975, professor Ken Walters published *Rheometry* [18], the first book dedicated exclusively to the measurements procedures of the rheological properties of non-Newtonian fluids. In Introduction, the author presented one main objective of this discipline (which is working in “tandem” with rheological modeling and numerical simulations [19,20]): “to determine the behavior of

<sup>☆</sup> Dedicated to Prof Ken Walters FRS on the occasion of his 80th Birthday.

<sup>\*</sup> Corresponding author. Tel./fax: +40 21 4029865.

E-mail address: [corneliu.balan@upb.ro](mailto:corneliu.balan@upb.ro) (C. Balan).

non-Newtonian liquids in a number of simple flow situation using suitable defined material functions” [18].

To fulfill this objective it is necessary not only to find general/universal solutions for the equation of motion, but also to impose proper boundary conditions for the working domain. However, in rheometry (especially for complex fluids) it is difficult to always put well posed boundary conditions, since the viscoelastic solutions might need “more boundary conditions than are supplied by the no-slip condition” [18].

In rotational rheometry (in particular plate–plate configuration) the boundary conditions are directly related to the fluid behavior at the walls (adherence or slip) and to the shape of the free surface at the edge of the plates (which is aprioric unknown). If the no-slip condition is normally accepted at the plates (considered to be perfectly smooth surfaces), it is almost impossible to control the boundary condition at the edge of the geometry.

Ken Walters inferred the importance of boundary conditions in rheometry and their direct connection to the quantification and interpretation of the experimental errors; in consequence, each of the chapters from *Rheometry* includes a paragraph dedicated to the analysis and discussion of *possible sources of errors*.

In the present paper we are mainly concerned with two categories of errors mentioned by Ken Walters in Ref. [18]: (i) edge and end effects, respectively (ii) instrument imperfections. Both are related with the fact that boundary of the flow domain is not precisely defined, and this is not referring only to the unknown free surface at the edge of the plates, but also with the deviation of the real geometry of the plates from the calculus geometry (due to misalignment, lack of parallelism, tilted axes).

We shall refer to these errors as end/edge effects and gap errors; we suppose that no-slip condition to solid walls holds and the free surface between the plates is cylindrical and in contact with the atmospheric pressure. End effects include inertia influence in a finite geometry (onset of secondary flows) and the error induced by the approximation of the real free surface of the sample at the edge with a cylindrical surface. Gap error is considered to be generated mainly by the non-parallelism of the plates, so the real gap is not constant along the surfaces. Since the goal of the work is to investigate the influence of pattern plates on the measurements in plate–plate geometry, it is compulsory to evaluate first the contribution of the end effects and gap error on the experiments performed for the smooth (commercial) plates, see Refs. [21–23].

The structure of the paper is the following: Section 2 is dedicated to the characterization of fluid samples and the measurements of the torques in simple shear for the smooth and patterned surfaces. A presentation of the surfaces microgeometry is also made. In Section 3 the gap error is analyzed in relation to a thin film (lubrication) analytical Stokes solution for rotational non-parallel surfaces. The results from numerical simulations of Newtonian and generalized Newtonian fluids (Carreau model) in plate–plate smooth and patterned configurations are shown in Section 4. Finally, in Section 5 the experimental and numerical results are analyzed and the conclusions of the work are presented.

## 2. Experimental

The investigations are performed with the Anton Paar Physica MC301 rheometer in controlled strain mode using the parallel plates configuration with diameters of 25 mm, respectively 50 mm, at constant temperature within a range from 10 °C to 25 °C. The reference values for the samples shear rheology are obtained using the cone and plate configuration (cone diameter of 50 mm and 1° angle). In experiments the upper plate was always the regular commercial stainless steel plate. Several lower plates of different materials and patterns have been tested: (i) current lower

plate of the rheometer (PN-plate), (ii) perfectly smooth silicon plate (Si-plate), (iii) silicon plate with pillars pattern (Si-pillars), (iii) copper alloy plate with microchannels pattern (channels plate).

Silicon wafers of 76 mm in diameter were processed at the IMT Bucharest (National Institute for Research and Development in Microtechnologies) using photolithography and DRIE (Deep Reactive Ion Etching) techniques to produce surfaces with pillars pattern, see also Ref. [24]. The plates patterned with parallel microchannels were obtained by classical mechanical procedure, see Fig. 1.

The most difficult part of the experimental protocol was to obtain a working set-up with minimum alignment and parallelism errors of the lower plates, relative to the rotational upper geometry plate. First, the horizontal position of the original lower plate was adjusted and the calibration to some prescribed gaps between the plates was performed using the measurements in three points of normal force between the upper plates and the feeler gauges of 50  $\mu\text{m}$  and 100  $\mu\text{m}$  (nominal height) mounted on the lower plate. The zero gap corresponds to the position where the measured normal (axial) force against the upper plate is zero. Therefore, in our case the prescribed nominal gap of the rheometer indicates actually the lowest gap height between the plates.

Each manufactured lower plate is fixed on the rheometer lower plate and the described calibration was performed before starting a new measurement. However, this procedure did not eliminate the lack of parallelism between the tools and the misaligned plate–plate problem generated by the gap variation along the contact surfaces. Using a set of feeler gauges of 40  $\mu\text{m}$ , 50  $\mu\text{m}$ , 60  $\mu\text{m}$ , 70  $\mu\text{m}$ , respectively 150  $\mu\text{m}$  and 160  $\mu\text{m}$ , we measured a gap difference between opposite edges of the 25 mm plate diameter of approximate 10  $\mu\text{m}$  (for all nominal gaps magnitude).

The samples used in experiments are two Newtonian liquids: Si-oil (silicone oil, with nominal viscosity of 0.4 Pa s at 20 °C) and En-oil (10W50 engine oil, with nominal viscosity of 0.4 Pa s at 10 °C and 0.275 Pa s at 20 °C), and a PIB-solution, a weakly elastic polymer solution of polyisobutylene with  $M_w = 0.5$  mil. (from Sigma Aldrich) in En-oil, with zero shear viscosity of 1.55 Pa s at 10 °C and 0.9 Pa s at 20 °C.

The reference temperature for each test and fluid was fixed as function of the measured temperature of the patterned lower plate. This temperature cannot be strictly controlled by the Peltier system of the rheometer, in consequence the shown data are obtained at different temperatures.

The oscillatory shear test of PIB-solution is presented in Fig. 2. The measured data disclose two phenomena: (1) the decreasing of the measured viscosity with reducing the gap in plate–plate configuration (so called the gap error effect), and (2) the influence of the lower plate quality on the measured torque. The first phenomena is well known in simple shear rheology and was recently investigated and analyzed in relation to the shear rheometry at high rates [25–28], see also Refs. [21–23]. The influence of the plate quality (assuming the plate is smooth) is determined by the adherence of the fluid at the material surface and possible slip occurrence. In Fig. 2 the measured differences in complex viscosity between the PN-plate and Si-plate are up to 20%, for the same value of the gap.

The samples (Newtonian liquids and PIB-solution) are not expected to exhibit significant slip at the walls of commercial plates. However, the measurements performed with perfect smooth Si-plates indicate possible presence of slip for PIB-solution in plate–plate geometry, the phenomenon which seems to be absent in the cone–plate configuration (where the recorded data are in the range of the experimental errors for the two tested smooth lower plates).

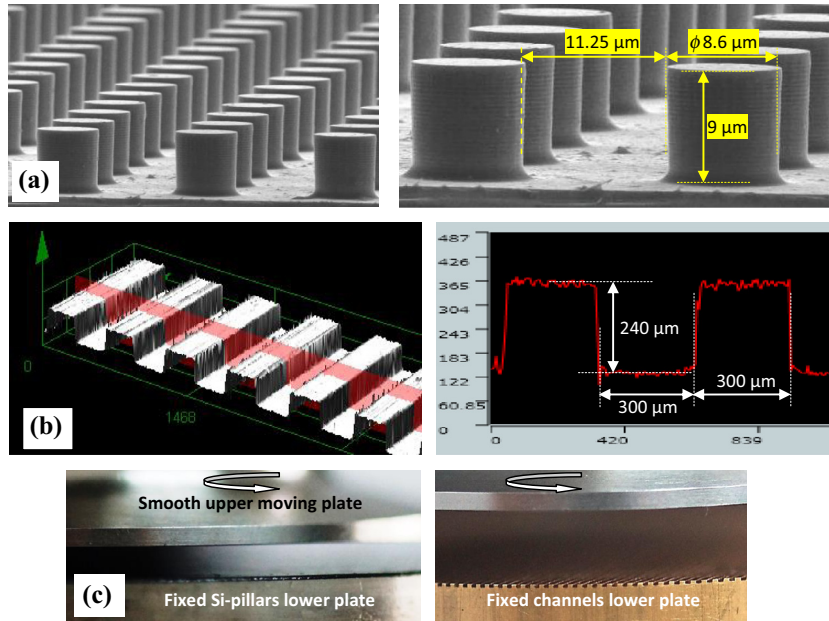


**Fig. 1.** The patterned plates used in experiments: (a) silicon pillars plate with uniform distribution of cylindrical pillars on the surface (by courtesy of IMT Bucharest), (b) channels plate (by courtesy of TU Darmstadt). The average dimensions of micro-geometries and the working setups are also shown (c).

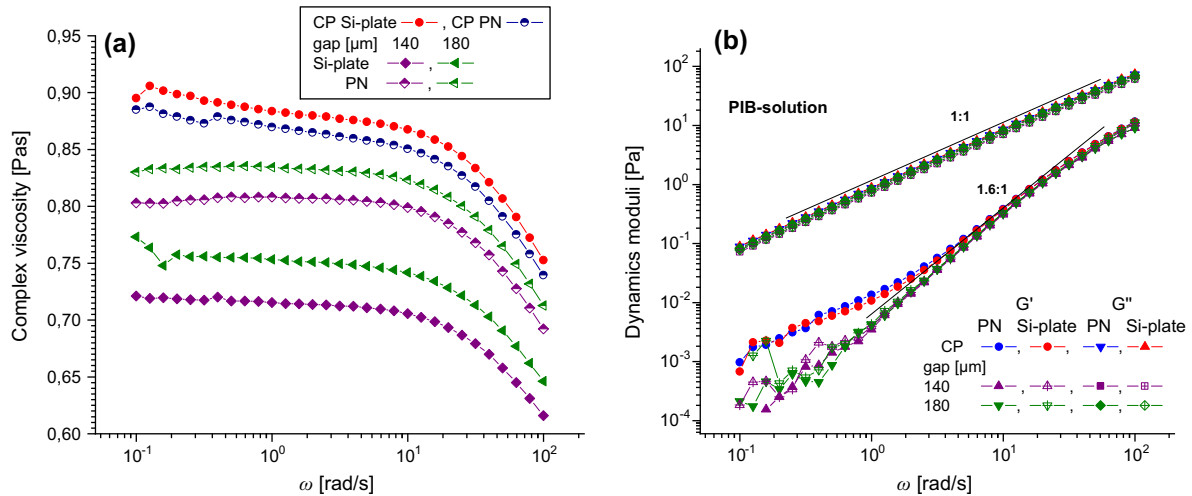


**Fig. 2.** The dependence of the complex viscosity (a) and the dynamics moduli of the PIB-solution (b) on the gap height and the quality of the smooth lower plate. Testes performed in oscillatory controlled strain frequency sweep at 0.1 [–] strain amplitude at 20 °C, with upper plate diameter of 50 mm. The reference measurements are obtained with cone and plate geometry (CP); the slopes of increasing  $G'$  and  $G''$  with frequency  $\omega$  are shown.

The gap error effect in torsional (plate–plate) flow is associated to the decreasing of the measured viscosity as the gap height  $h$  is decreasing. This phenomenon is generated by the geometrical non-conformity of the working configuration in comparison to the ideal geometry used in computations. In particular, the error is mainly induced by the non-parallelism of the plates. In this case the gap height is not homogeneous between the plates (as we have already reported). The zero gap procedure indicates the lowest value of the gap height, same value being used to command the rim shear rate. In consequence, the measured torque  $T_m$  will be less than the theoretical torque  $T_t$  because the real gap is actually larger than the imposed one.

The theoretical torque in plate–plate configuration is considered to be identical with the corresponding torque in a steady torsional flow of an equivalent Newtonian fluid with viscosity  $\eta_0$ ,

$$T_t = \frac{\pi\omega R^4}{2h} \eta_0, \quad (1)$$

where  $\omega$  is the relative angular speed between the plates,  $R$  is the radius of the plates and  $h$  is the constant height of the gap.

In experiments, the measured shear stress  $\sigma_R$  and the commanded shear rate  $\dot{\gamma}_R$  are calculated with the relations

$$\sigma_R = \frac{2T_m}{\pi R^3}, \quad \dot{\gamma}_R = \frac{\omega R}{h}, \quad (2)$$

the computed viscosity function being defined as:

$$\eta := \frac{\sigma_R}{\dot{\gamma}_R}. \quad (3)$$

The formula of the shear rate in Eq. (2)<sub>2</sub> is valid only for perfectly smooth parallel plates. For non-parallel discs or patterned plates the value of  $\dot{\gamma}_R$  represents an apparent shear rate because the local flow is no more a homogeneous pure shear in the gap (especially for lower patterned surfaces).

Relations (1) and (2) are valid for no-slip boundary conditions and do not take into consideration neither the end-effects (the

plates are considered infinite), the inertia influence (Reynolds number tends to zero) nor the Weissenberg correction [13,18].

We have to mention that Weissenberg correction (represented by the term  $\partial \ln \sigma_R / \partial \ln \dot{\gamma}_R$  applied to (2)<sub>1</sub> is not related to the gap effect, but with the non-linearity of the viscosity function (if  $\partial \ln \sigma_R / \partial \ln \dot{\gamma}_R = 1$  the formula (2)<sub>1</sub> is correct), see Fig. 3.

The gap error effect, induced by the lack of parallelism between the plates, on the computed viscosity (3) becomes more relevant as the gap is smaller and the fluid viscosity is lower. Some other phenomena which may influence the calculation of viscosity (the end-effects, inertia, Weissenberg correction for the shear stress at the rim in the non-linear viscoelastic regime) cannot explain the recorded relatively large differences between the measured viscosity at different gaps in the plate–plate configuration, especially at  $h < 0.2$  mm, see for details Refs. [21,23].

The influences of gap and patterned surface in simple shear of PIB-solution and En-oil for a Si-pillars and channel plate patterned surfaces are presented in Figs. 4 and 5 (the effect of microgeometry on the measurements in plate–plate rheometry was previously reported by the authors in Ref. [29]).

All performed experiments in shear (different samples, temperatures and shear rates) confirm that, at the same apparent shear rate, the measured viscosity is decreasing by decreasing the gap height. We also recorded lower values of the measured viscosity for patterned plate as compared to the values measured viscosity for smooth (normal) plate, at the same gap and same apparent shear rate.

The difference between smooth and patterned surfaces are also noticed during stress relaxation of PIB-solution. For smooth plates stress relaxes almost immediately to zero at any gap; for patterned plates the relaxed shear stress reaches fast a small but constant residual stress, its value being increased by decreasing the gap, see Fig. 6.

The experimental investigations in shear are summarized in Fig. 7, where the measured viscosity as function of gap is represented for different lower plate quality and microgeometries at the apparent shear rate of  $50 \text{ s}^{-1}$ .

### 3. Gap influence

The gap error in plate–plate geometry is remarkable for nominal gaps below about  $200 \mu\text{m}$ . The phenomenon was probably the first time investigated in Ref. [21] and in the last decade several studies on the gap error were published by Stokes et al., e.g. Refs. [22,23,25], in the most recent one being proposed a GLM

(generalized linear model) methodology to analyze the experimental data and estimate the gap error [23]. The subject has become of interest especially in relation with the novel procedures to measure rheological properties at high and very high shear rates based on the microgap rheometry, see Refs. [25–28].

In classical shear rheometry is generally accepted to represent the gap error by dimension  $h_e$  defined as:

$$h_e = h \left( \frac{\eta_0}{\eta_m(h)} - 1 \right), \quad (4)$$

where  $h$  is the prescribed gap (the input value for the rheometer, also the value used to compute the apparent shear rate  $\dot{\gamma}_R$ ) and  $\eta_m(h)$  is the measured viscosity (3) for the imposed shear stress (2)<sub>1</sub> [21,23]. The gap errors (4) are calculated for our data and the values  $h_e(h)$  are shown in Fig. 8.

In Fig. 8 the reference value for  $\eta_0$  is given by the measurement in cone-plate configuration. In all cases, within an experimental error of  $\pm 2\%$ ,  $\eta_0$  almost coincides with the viscosity measured in plate–plate geometry for  $300 \mu\text{m}$  gap.

The calculated dimension  $h_e$  in (4) does not really represent the true error in the measurement of the gap; it is just a “virtual dimension” added to  $h$  in order to calculate accordingly to (3) the correct viscosity (at given velocity of the upper plate and the measured  $\sigma_R$ ).

In the case of a fluid with constant viscosity, no-slip conditions and smooth plates surfaces, in the value of  $h_e$  include 3 types of errors: (i) gap error (lack of plates parallelism/misalignment, which is considered to be dominant), (ii) end/edge effect (the real edge surface of the sample is not cylindrical), (iii) inertia/presence of secondary flows ( $Re$  number influence).

The effect of patterned surfaces observed in our tests (see Figs. 7 and 8, for example) is not generated by the one of these phenomena. The influence of surface quality on the measurements is investigated and analyzed in the next paragraph using the results of numerical simulations of the flow field in the gap.

In the absence of the complete 3D topography of the plates and accurate 3D measurements of plates misalignments, the gap error can be explained, and to some extent even computed, using the thin film theory [30,31].

The velocity distribution in a thin film of a Newtonian fluid between two non-parallel discs of radius  $R$  and gap  $h \ll R$ , see Fig. 10, is approximated by the relation,

$$v = \frac{1}{2\eta_0 r} z(z-h) \frac{\partial p}{\partial \varphi} + r\omega \frac{h-z}{h}, \quad (5)$$

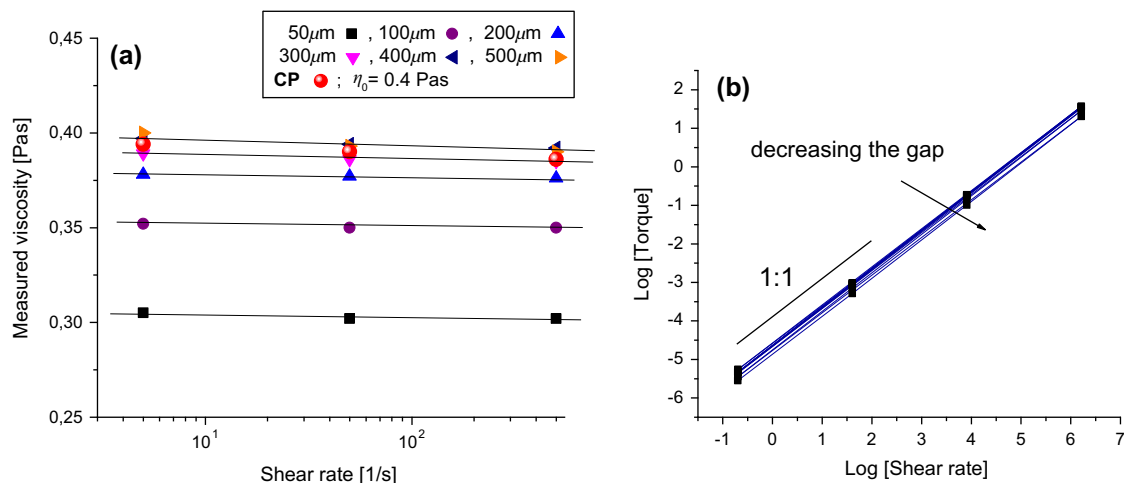
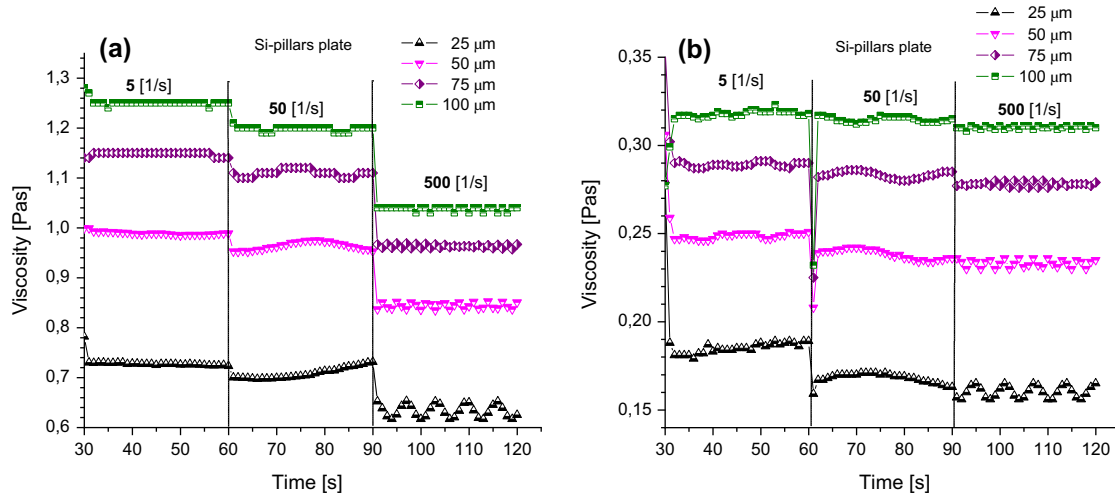
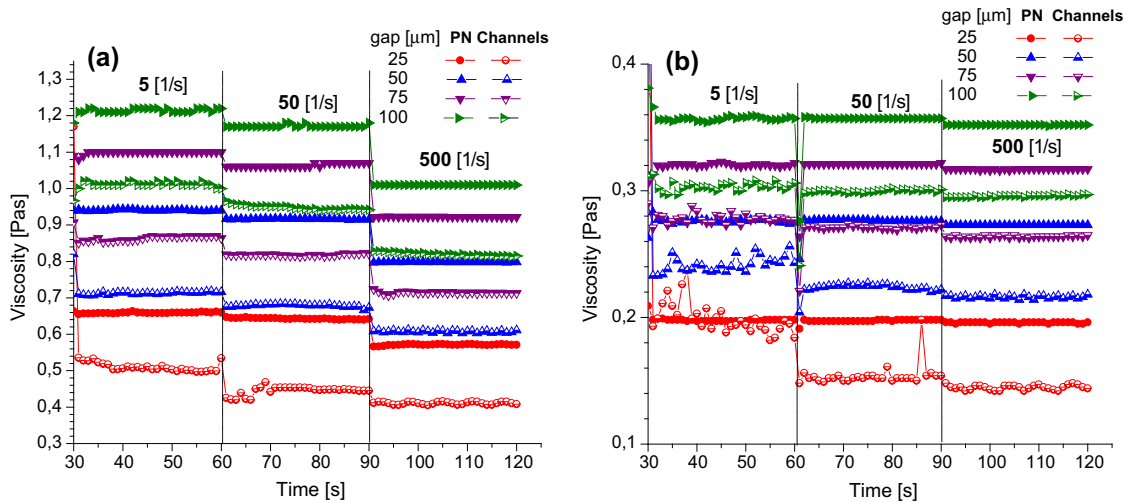


Fig. 3. The gap error effect in shear: (a) measured viscosity as function of the gap magnitude; (b) the Weissenberg correction coefficient is equal to one (Si-oil, PN-plate, upper plate diameter of 50 mm, 20 °C).



**Fig. 4.** The gap influence; measured viscosity at constant apparent shear rate ( $5 \text{ s}^{-1}$ ,  $50 \text{ s}^{-1}$ ,  $500 \text{ s}^{-1}$ , respectively) for PIB-solution (a) and En-oil (b) at  $10 \text{ }^\circ\text{C}$  (Si-pillars pattern lower plate; upper plate diameter of 25 mm).



**Fig. 5.** Patterned surface and gap influences; measured viscosity at constant apparent shear rate ( $5 \text{ s}^{-1}$ ,  $50 \text{ s}^{-1}$ ,  $500 \text{ s}^{-1}$ , respectively) for PIB-solution (a) and En-oil (b) at  $15 \text{ }^\circ\text{C}$ ; comparison between the normal lower plate and the channels pattern lower plate (upper plate diameter of 25 mm).

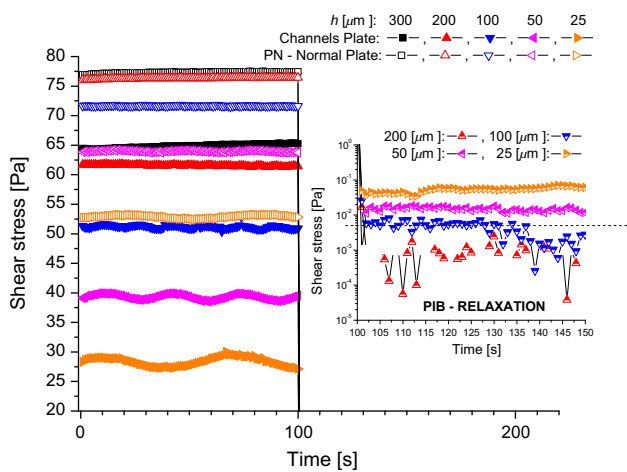


**Fig. 6.** The patterned surface and gap influences; shear stress vs. time followed by relaxation for PIB-solution at  $\dot{\gamma} = 50 \text{ s}^{-1}$  (temperature  $10 \text{ }^\circ\text{C}$ , upper plate of 25 mm). The lower limit of the torque transducer corresponds to the shear stress value of 5 mPa, below this value some oscillations of the shear stress are observed.

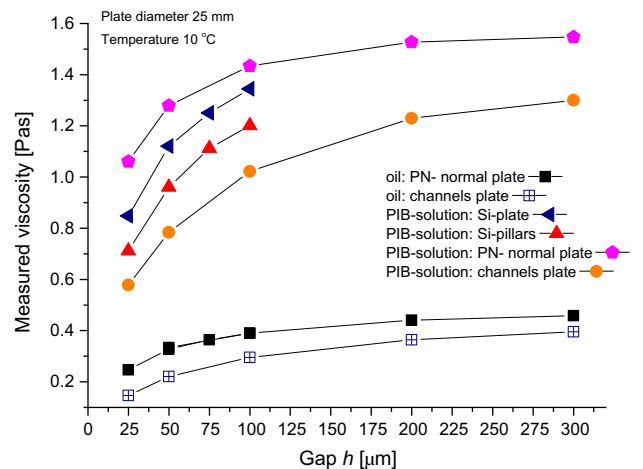


**Fig. 7.** The gap and patterned surface influences on the measurement of shear viscosity in plate and plate geometry at constant shear rate  $\dot{\gamma} = 50 \text{ s}^{-1}$  for En-oil and PIB-solution.

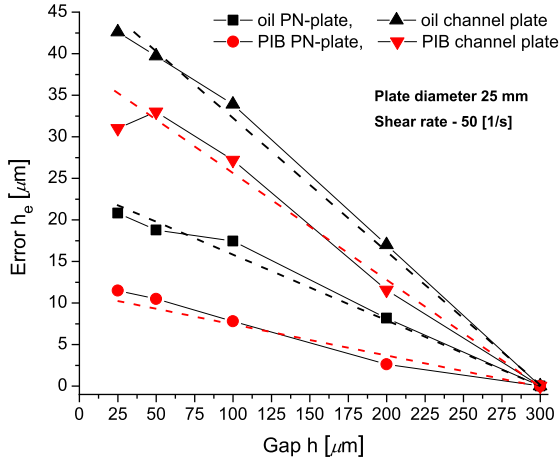


**Fig. 8.** The gap error at constant shear rate for En-oil and PIB-solution (PN-plate and channel plate), see Fig. 7. The error  $h_e$  is much larger for the patterned channel plate in comparison with the smooth normal plate.

where  $\omega$  is the constant relative angular velocity between the plates,  $v = v_\varphi(r, z)$  is the rotational velocity and  $\eta_0$  is the fluid viscosity.

Relation (5) is directly obtained from the integration of the Navier–Stokes equation in the limit of zero Reynolds number, with  $v_r, v_z \ll v_\varphi$ .

The pressure distribution in the gap is obtained from the integration of the continuity equation, i.e.  $\int_0^h \partial v / \partial \varphi dz = 0$ , respectively as solution of Riccati equation

$$p'' + \frac{3}{h} p' + \frac{k}{h^3} = 0, \quad (6)$$

where  $p = p(h)$ , for  $h \in [h_1, h_2]$  with  $h = h_1 - \frac{\varepsilon}{\varphi_0} \varphi$ , for  $\varphi \in [0, \varphi_0]$ ,  $\varepsilon = h_1 - h_2$  and  $k = \frac{6\eta_0 r^2 \omega \varphi_0}{\varepsilon}$ , see Fig. 9.

Relation (6) is reduced to the equation  $p' = \frac{C}{h^3} - \frac{k}{h^3}$ , with  $C = 2k \frac{h_1 h_2}{h_1 + h_2}$ , and the relative pressure distribution within the gap is:

$$p = \frac{6\eta_0 \omega r^2 \varphi_0}{\varepsilon} \left( \frac{1}{h} - \frac{1}{h_1 + h_2} - \frac{1}{h^2} \frac{h_1 h_2}{h_1 + h_2} \right), \quad (7)$$

where  $p = 0$  for  $h = h_1$  and  $h = h_2$ .

The shear stress acting on the upper plate is calculated with the formula,

$$\begin{aligned} \sigma &= \eta_0 \frac{\partial v}{\partial z} \Big|_{z=h} = \eta_0 \frac{r\omega}{h} + \frac{\varepsilon h}{2r\theta_0} p' \\ &= \eta_0 \frac{r\omega}{h} \left( 1 + 3 \left( \frac{2h_1 h_2}{h(h_1 + h_2)} - 1 \right) \right), \end{aligned} \quad (8)$$

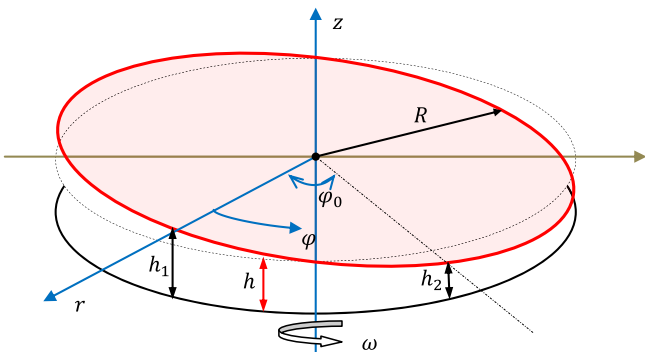


**Fig. 9.** Non-parallel plate–plate configuration with variable gap  $h$ .

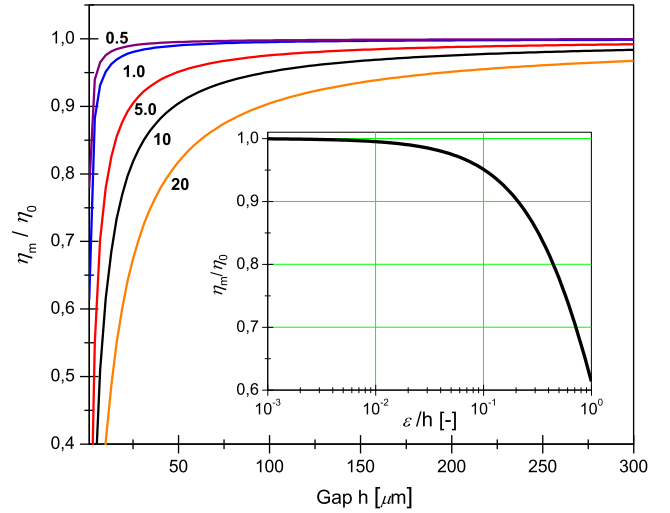


**Fig. 10.** The correction function  $\kappa(x)$  and its variation with the gap for different values of  $\varepsilon$  [ $\mu\text{m}$ ].

and the torque (2)<sub>1</sub> is computed by the relation,

$$T^* = \frac{\varphi_0}{\varepsilon} \int_0^R \int_{h_1}^{h_2} \sigma r^2 dr dh, \quad (9)$$

respectively, for  $\varphi_0 = 2\pi$  and  $x = \varepsilon/h_2$ , the shear stress at the rim of the plate becomes:

$$\sigma_R^* = \frac{2T^*}{\pi R^3} = \kappa(x) \cdot \eta_0 \dot{\gamma}_R, \quad (10)$$

where

$$\kappa(x) = 2 \left( -\frac{1}{x} \ln(1+x) + \frac{3}{2+x} \right). \quad (11)$$

The expression (11) is the correction function for the computed/measured viscosity (3), i.e.  $\kappa(x) = \eta_m / \eta_0$ , if the two plates are not parallel ( $\kappa(x) = 1$  for  $x = 0$ , respectively for  $h_1 = h_2$ ), see Fig. 10. We have to remark that in experiments the input nominal gap  $h$  is given by the values of  $h_2$ .

Relations (7)–(11) are found in classical books of fluid mechanics as particular solution of the Reynolds lubrication equation for slider bearings [32,33], but here the solution is obtained by direct integration of the Newtonian thin film flow in cylindrical coordinates.

This calculus is qualitatively relevant for our study because it proves that non-parallelism of the plates in rotational rheometer, represented by the value of  $\varepsilon$ , generates a lower measured viscosity than expected, as the nominal gap  $h = h_2$  is decreasing. Relation (11) and the diagrams from Fig. 10 might also offer a quantitative correction of the measured viscosity  $\eta_m$ . This result is explored in the next sections of the paper, considering the measured value  $\varepsilon = 10 \mu\text{m}$  for the gap difference (value reported in §2).

#### 4. Numerical simulations

Numerical solutions for the plate–plate geometry, respectively plate–channels geometry, were obtained using the commercial Fluent code for the Newtonian fluid and Carreau model,

$$\frac{\eta(\dot{\gamma}) - \eta_\infty}{\eta_0 - \eta_\infty} = \left[ 1 + (\lambda \dot{\gamma})^2 \right]^{\frac{n-1}{2}}, \quad (12)$$

where  $\dot{\gamma}$  is the local shear rate,  $\eta_0$  is zero shear viscosity,  $\eta_\infty$  is the infinite viscosity,  $n$  is the shear thinning exponent and  $\lambda$  is the time

constant. The Carreau model is one of the most versatile and common relation to represent the shear thinning behavior with a continuous and derivable viscosity function between finite limits ( $\eta_0$ , respectively  $\eta_\infty$ ).

Fluent is a robust code which solves the Navier–Stokes flows with constant or variable viscosity using the finite volume technique. The simulations were performed using the steady viscous laminar solvent with SIMPLE (semi-implicit method) algorithm for pressure–velocity coupling and second order discretization. The relative convergence error is  $10^{-8}$  for the equation of continuity and velocity components.

The input viscosities for the Newtonian flows were  $\eta_0 = 1.06$  Pa s and  $\eta_0 = 0.1$  Pa s and the Carreau model was defined by the following constants:  $\eta_0 = 1.06$  Pa s,  $\eta_\infty = 1.0$  mPa s,  $\lambda = 10$  s and  $n = 0.7, 0.2$  and  $-1$ , respectively.

Solutions are obtained for the plate diameter  $d = 25$  mm at different gaps in the range  $25 \mu\text{m} \leq h \leq 300 \mu\text{m}$ . The upper plate is rotated with constant speed, corresponding to the shear rate  $(2)_2$  in the interval  $\dot{\gamma}_R \in [10^{-2} \div 10^3] \text{s}^{-1}$  and the lower plate is at rest. The rotational plate has always been considered smooth and the lower plate has been taken to be smooth or patterned with channels geometry (see Fig. 1(b and c)). No-slip boundary condition is imposed at the plates surface and the edge of the geometry is considered a cylindrical surface at constant pressure.

The grid was built based on uniform distributed hexahedral similar mesh cells for all configurations, so the number of nodes varies with the gap and type of geometry (normal or channel plate) between 2 and 3 million, with the remark that density of the nodes (respectively cells) was increasing at the edge of the plates. The channel geometry was discretized with quad-elements (type map), respectively tri-elements (pave type) were used to mesh the upper moving plate.

One of the aim of the simulations was to compute the torque acting on the upper plate of the PN geometry ( $T_m = T_c$ ) and to compare the input viscosity,  $\eta_0$  or viscosity function (12), to the

calculated viscosity from (3). The results for the Newtonian fluid from Tables 1 and 2 correspond to  $\dot{\gamma} = 1 \text{s}^{-1}$  (the ratio  $T_c/T_t$  being almost identical for the whole range of simulations).

The results from Table 1 show that end-effect is less important in 3D than in 2D computations, however the error represented by the ratio  $T_c/T_t$  is decreasing by decreasing the gap, see Table 2. The end-effect is determined by the imposed boundary condition for pressure, which induces a secondary flow in the vicinity of the plate edge and an increase in the local wall shear stress, see Fig. 11. Hence, the calculated viscosity from numerical simulations is always higher than the input viscosity.

If the reference value for torque is considered at a precise value of the gap (e.g.  $h = 200 \mu\text{m}$ ), then the relative measured torque  $T_c/T_{200}$  (and in consequence, the measured viscosity) is monotonically decreasing by the gap magnitude, see Table 2. This phenomenon is not present in the “infinite geometries” and is a measure of the influence of the end/edge effect with reducing the gap. However, this effect is always observed in experiments where the end-effect cannot be avoided.

In reality, the decrease of the measured viscosity by the decreasing of the gap is more significant than the numerical results from Table 2 show, due to the gap error effect.

Indeed, the simulations of the rotational flows between non-parallel (oblique) plates for  $\varepsilon = 10 \mu\text{m}$  and  $\alpha = 0.1$  ( $h = 100 \mu\text{m}$ ), respectively  $\alpha = 0.2$  ( $h = 50 \mu\text{m}$ ), confirm the analytical results from relation (11), see Table 3. The simulations at  $\dot{\gamma} = 10\text{s}^{-1}$  generate very similar values for the correction factor, so we are confident to consider that  $\kappa$  is independent on the apparent shear rate.

The wall shear stress (WSS) distributions on the diameters of the upper and lower plates are represented in Fig. 12 for perfect parallel plates and tilted (oblique) configuration. In the last case the non-symmetric stress distribution justifies the lower measured torque than in the case of perfect alignment plates.

The analysis of the two effects: (i) end effect (due to secondary flows), and (ii) gap error (due to the gap non-homogeneity) in rela-

**Table 1**  
Theoretical and computed torques at  $h = 100 \mu\text{m}$  and  $\dot{\gamma} = 1 \text{s}^{-1}$ .

Theoretical torque $T_t$ ( $\mu\text{N m}$ )	2D axial-symmetric (finite)		2D axial-symmetric (infinite)		3D geometry	
	$T_c$	$T_c/T_t$	$T_c$	$T_c/T_t$	$T_c$	$T_c/T_t$
3.25204	3.49107	1.07	3.25204	1.0	3.35398	1.03

**Table 2**  
End-effect and gap influences: 2D axial-symmetric and 3D simulations at  $\dot{\gamma} = 1 \text{s}^{-1}$ . The reference value for the torque,  $T_{200}$ , is taken a gap of  $200 \mu\text{m}$ .

$h$ ( $\mu\text{m}$ )	200		100		75		50		25	
	2D	3D	2D	3D	2D	3D	2D	3D	2D	3D
$T_c/T_t$	1.176	1.07	1.07	1.03	1.05	1.018	1.034	1.009	1.013	1.003
$T_c/T_{200}$	1	1	0.913	0.96	0.893	0.945	0.88	0.934	0.86	0.93

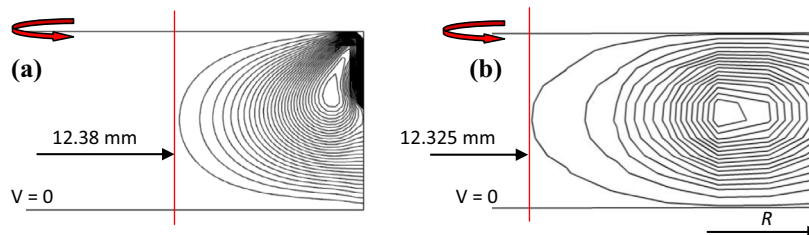


**Fig. 11.** The end-effect; the spectrum of the computed radial velocity at the edge of the plates: (a) 2D simulation, (b) 3D simulation (Newtonian fluid, smooth geometry,  $R = 12.5$  mm,  $h = 100 \mu\text{m}$  and  $\dot{\gamma} = 1 \text{s}^{-1}$ ).

**Table 3**

Computed torques for the normal parallel plates  $T_{cPN}$  and for the oblique plates  $T_{co}$ ;  $\kappa$  is the correction factor from (11) and  $\kappa_n$  is the value calculated from numeric with  $\epsilon = 10 \mu\text{m}$  ( $d = 25 \text{ mm}$ , apparent shear rate  $\dot{\gamma} = 1 \text{ s}^{-1}$ ,  $\eta_0 = 1.06 \text{ Pa s}$ ).

$h$ ( $\mu\text{m}$ )	100	50
$T_{cPN}$ ( $\mu\text{N m}$ )	3.354	3.283
$T_{co}$ ( $\mu\text{N m}$ )	3.188	2.983
$\kappa$	0.95	0.908
$\kappa_n$	0.95	0.9

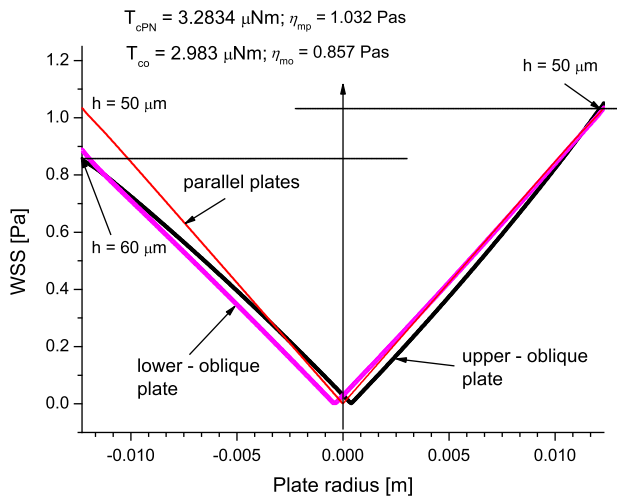


**Fig. 12.** Wall shear stress distribution on the diameters of the plates for  $h_1 = 60 \text{ mm}$  and  $h_2 = 50 \text{ mm}$ , see Fig. 9 and Table 3.

tion to the experimental data for smooth and pattern surfaces is presented in the last section of the paper.

Simulations for the 3D configuration where the lower plate is patterned with channels, see Fig. 1(b), are performed only for parallel plates. The results disclose the oscillations of the computed wall shear stress in the gap (due to the presence of the channels on the lower plate) and lower values of WSS than the correspond-

ing normal smooth configurations for the Newtonian fluid and Carreau models with positive  $n$  – exponent, see Figs. 13–15.

The numerical simulations offer the possibility to get important details not only on the kinematics of secondary flows in the microchannels, see Figs. 16 and 17, but also on the viscosity distribution in the gap for the shear thinning fluids, Fig. 18. In Figs. 16 and 17 some of the trajectories exit from the gap. This phenomenon is an effect of numerical errors due to the imposed boundary conditions at the edge of the plates corroborated with the mesh quality (the mesh density being imposed by the available computation capacity). However, the computed flow rate exiting from the gap is of order of  $10^{-10} \mu\text{g/s}$  and the transported flow rate has the order of  $1 \mu\text{g/s}$ , so the influence of this error is very limited and affects the kinematics only in the very vicinity of the gap rim.

The quantitative comparison between the computation for smooth and patterned plates (with no-slip boundary conditions) sustains the concept of the apparent slip at microgrooved walls, which has to be distinguished from the effective slip observed at microstructured surfaces [34–36], see also Ref. [37]. The numerical results and the experimental data from §2 are analyzed in the next paragraph.

**5. Analysis and conclusions**

The first step in modeling the torsional flow between patterned surfaces has to be the correct representation of the flow dynamics in the corresponding smooth geometry. The problem needs a careful analysis when the results of the modeling (analytic or numeric) are compared to the experiments quantitatively. The real configuration of the tested geometry might be locally quite different from the assumed calculus geometry, and the discrepancy between the two configurations is most probably increasing by decreasing the gap. Such discrepancies may induce errors in the calculus of global parameters, as torque friction, and generate false conclusions on the fluid behavior at the boundaries of the plates.

Many applications of simple and complex flows in the presence of patterned surfaces are related to microfluidics and tribology. The major goal of the studies is to control the boundary conditions, to generate slip at the walls [38–40] or to create hydrophobic surfaces for reducing the drag [41,42]. Several microgeometries (pillars,

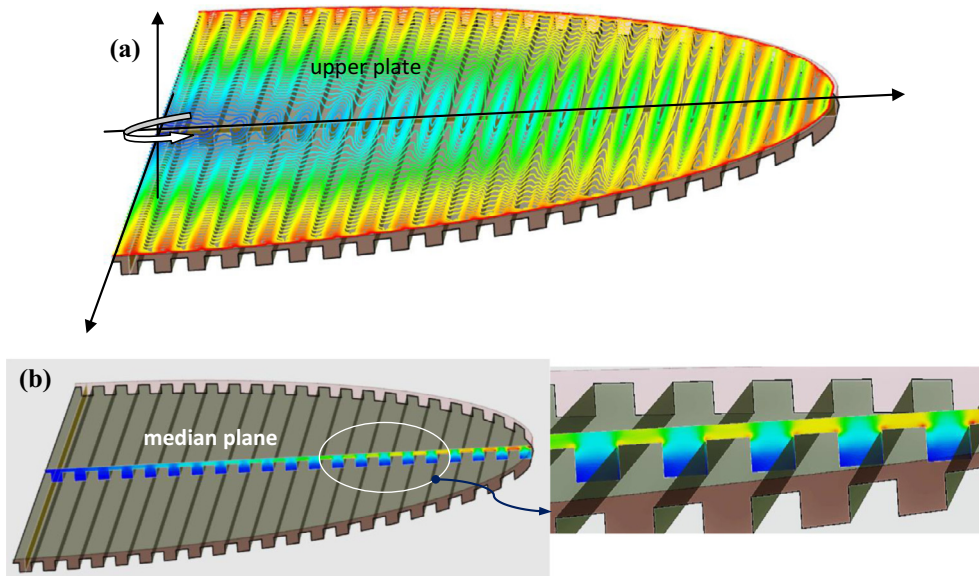


**Fig. 13.** Computed shear stress distribution for the Newtonian fluid (the values vary from blue color to red color, see Fig. 12 for the magnitude of WSS): (a) upper plate, (b) median plane with a detail ( $h = 100 \mu\text{m}$ ,  $\dot{\gamma} = 1 \text{ s}^{-1}$ ,  $\eta_0 = 1.06 \text{ Pa s}$ ). (For interpretation of the references to color in this figure legend, the reader is referred to the web version of this article.)

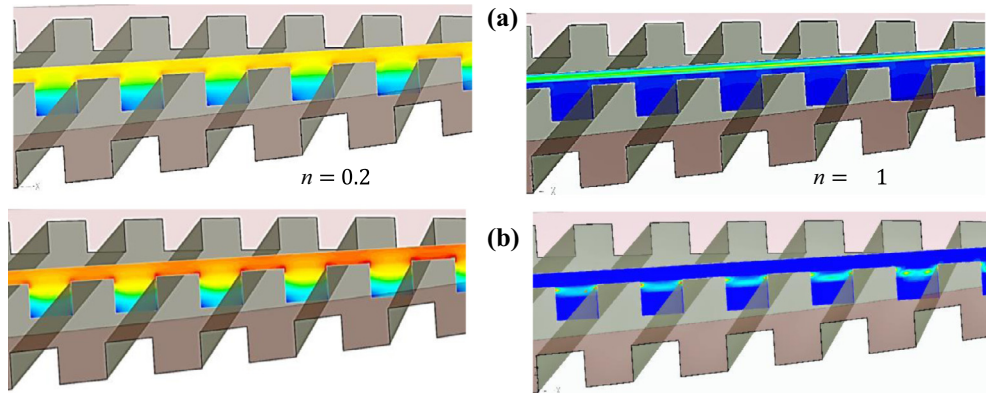


Fig. 14. Computed shear stress distribution for the Carreau models ( $n = 0.2$  and  $n = -1$ ) on the median plane: (a)  $\dot{\gamma} = 1 \text{ s}^{-1}$ , (b),  $\dot{\gamma} = 10 \text{ s}^{-1}$  ( $h = 100 \mu\text{m}$ ).

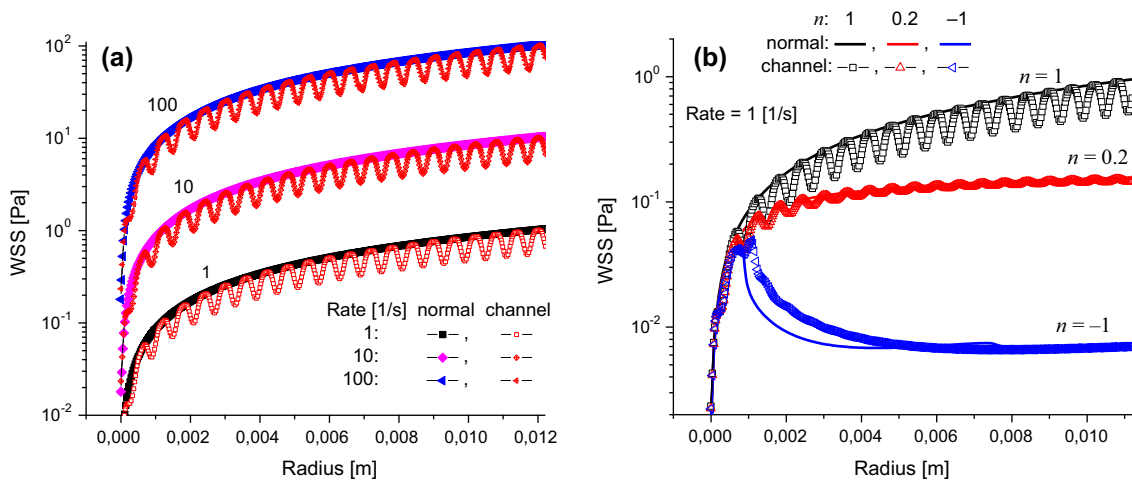


Fig. 15. Wall shear stress distribution on the diameter of the upper (moving) plate for  $h = 100 \mu\text{m}$ : (a) Newtonian fluid ( $\eta_0 = 1.06 \text{ Pa s}$ , apparent shear rate as parameter), (b) Carreau model ( $n$  - exponent as parameter).

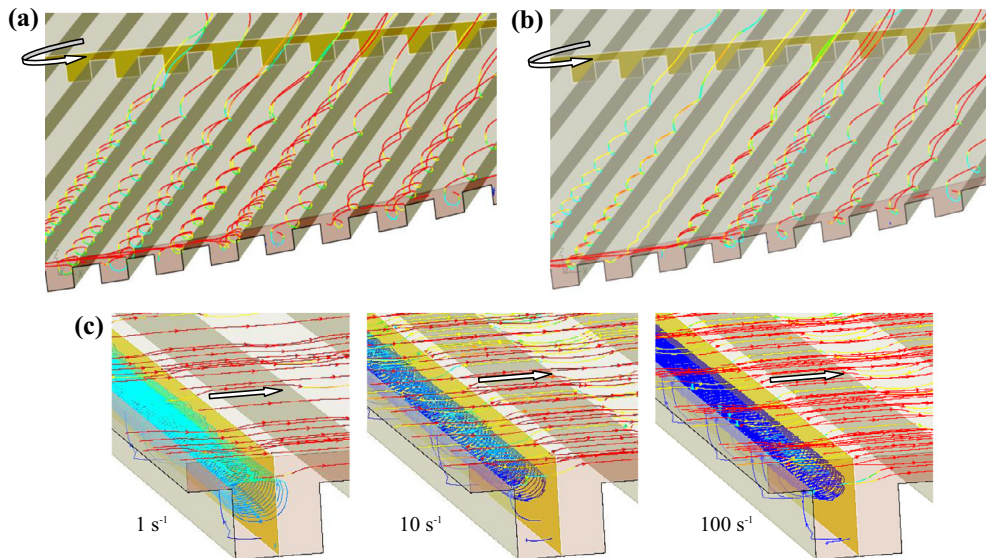


Fig. 16. Flow trajectories in the gap for the channels plate geometry (colored by the velocity magnitude): (a) Newtonian fluid  $\eta_0 = 1.06 \text{ Pa s}$ , (b) Carreau model with  $n = 0.7$  ( $h = 100 \mu\text{m}$ ,  $\dot{\gamma} = 10 \text{ s}^{-1}$ ); (c) details with the flow trajectories for the Carreau model with  $n = 0.2$  at  $\dot{\gamma} = 1 \text{ s}^{-1}$ ,  $\dot{\gamma} = 10 \text{ s}^{-1}$  and  $\dot{\gamma} = 100 \text{ s}^{-1}$ . (For interpretation of the references to color in this figure legend, the reader is referred to the web version of this article.)

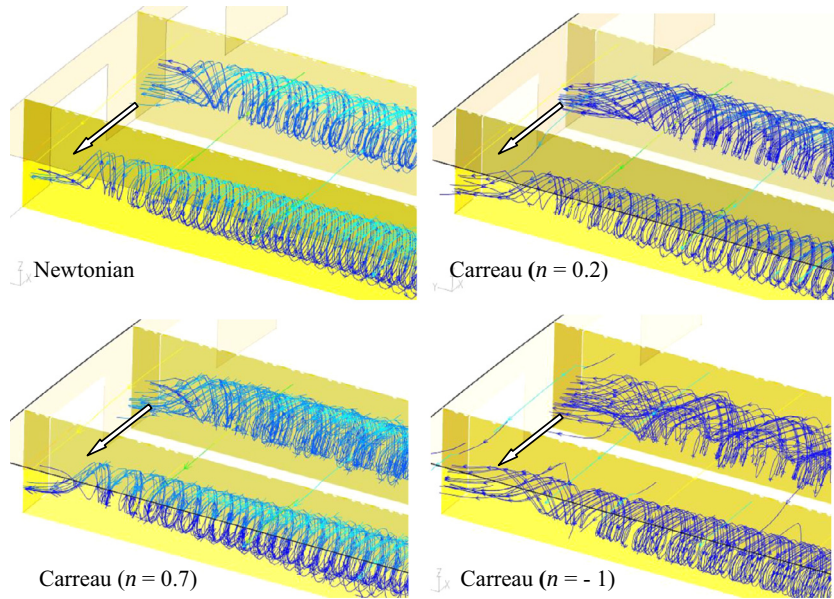


Fig. 17. Details of the secondary flow patterns in the channels of the lower plate for the Newtonian and the Carreau models ( $\dot{\gamma} = 1 \text{ s}^{-1}$ ).

$n$ - index	0.7	0.2	-1.0
Rate			
$\dot{\gamma} = 1 \text{ s}^{-1}$			
$\dot{\gamma} = 10 \text{ s}^{-1}$			

Fig. 18. Viscosity distribution in a channel for the Carreau model ( $n$  - exponent as parameter). Lower viscosity corresponds to the surface of the upper (moving) plate; shear banding phenomena is observed for negative  $n$ -exponents ( $h = 100 \text{ }\mu\text{m}$ ,  $\dot{\gamma} = 1 \text{ s}^{-1}$ ,  $\dot{\gamma} = 10 \text{ s}^{-1}$ ).

microgrooves, channels, strips) have been tested for those purposes. Since it is not easy to obtain a complete description of the flow kinematics in the vicinity of such surfaces, the target of the studies is to evaluate the hydrophobicity of a given surface pattern as function of the measured slip velocity.

But the observed slip velocity is not always the lack of adherence of the fluid to the solid wall. In many applications the lack of adherence is only apparent, the phenomenon being generated by wall depletion, shear banding or the presence of multiphase flows (i.e. the existence of the air in microgrooves).

The main aim of our work was to evaluate the contribution of the patterned surface on the measurements in plate-plate geometry and to give a quantitative representation of the experimental results. Firstly we have analyzed the contribution of the end effects and the gap error for smooth plates under no-slip boundary conditions. If the correction factor  $\kappa$  (which represent the contribution

of the gap error, see Table 3) is corroborated with the end-edge effect contribution from Table 2, one can compute the total relative measured torque  $-(T_c/T_{200})_T$  for the experiments performed in real conditions, e.g.  $(T_c/T_{200})_T = 0.90-0.934 \cong 0.84$  for nominal gap of  $h = 50 \text{ }\mu\text{m}$  and  $\varepsilon = 10 \text{ }\mu\text{m}$ . Consequently the measured viscosity at  $h = 50 \text{ }\mu\text{m}$  will be only 84% of the viscosity recorded at the gap of  $200 \text{ }\mu\text{m}$ . We notice that this result is not determined by any slip or lack of adherence at the plates surfaces.

Real or apparent slip might generate at macroscopic scale similar consequences with the non-parallelism of the plates (gap error) or with the presence of the micro-structures at the wall. The decreasing of torque in plate-plate rheometry for patterned surfaces in comparison with the smooth surface is such consequence, see Fig. 7. In Table 4 computed torques are presented at the upper plate (based on numerical simulations with no-slip boundary condition) for normal and channel lower plates ( $T_{cPN}$ ,

respectively  $T_{cch}$ ) and also the relative torque  $a_T = T_{cch}/T_{cPN}$ . Therefore, at the gap of 50  $\mu\text{m}$ , and the same apparent rate, we expect a decreasing in friction on the upper plate by 21% for patterned lower plate, phenomenon which is determined by the change in the flow kinematics within the gap, see Figs. 16 and 17.

A sketch of the simple shear flow in the vicinity of a smooth and patterned surface is represented in Fig. 19. Here  $b$  is the real slip length, with  $b^* = b + H$ , where  $H$  and  $d$  are the characteristic dimension of the microgeometry. The gap  $h$  and the applied velocity  $V_0^*$  on the upper plate is the same in both cases. We assume that at smooth surfaces the no-slip boundary condition is applied.

In the case of patterned plate (Fig. 19.b) we might have *real (effective) slip* at the wall (slip velocity  $V_{sw}$ ), slip at  $y = H$  (slip velocity  $V_s$ ) or *apparent slip* (velocity  $V_{as}$  at  $y = \delta$ ,  $\delta > H$ , with zero velocity at  $y = H$ ), which is associated to a high velocity gradient in the vicinity of the wall. In all cases the velocity distribution discloses the same value at  $y = \delta$  and identical patterns for  $y > \delta$ , so the real slip cannot be easily differentiated from the apparent slip.

One procedure to analyze the existence of slip at the wall is based on the definition of the *structural parameter*  $b^*$ ,

$$b^* = \left( \frac{\sigma_0^*}{\sigma_s^*} - 1 \right) h, \tag{13}$$

where  $\sigma_0^*$  is the measured shear stress at the upper plate of a smooth geometry and  $\sigma_s^*$  is the measured shear stress at the upper plate of a geometry with patterned lower wall [29], see also Refs. [34,35].

For a given microgeometry and  $\sigma_0^* > \sigma_s^*$ , the computation of  $b^*$  might characterize the *flow regime on patterned surface* relative to the flow at the smooth surface. A positive dimension  $b_r := b^* - H$  defines a flow regime with effective induced slip at the patterned surface; if  $b_r < 0$  the flow is associated to the apparent slip induced by the plate's microgeometry.

In the case of numerical simulations performed for the patterned channels pattern with  $H = 240 \mu\text{m}$ , the value of  $b_r$  is nega-

**Table 4**  
Computed torques for normal plate and channel plate ( $d = 25 \text{ mm}$ , apparent shear rate  $\dot{\gamma} = 1 \text{ s}^{-1}$ ,  $\eta_0 = 1.06 \text{ Pa s}$ ).

$h \text{ (}\mu\text{m)}$	100	75	50	25
$T_{cPN} \text{ (}\mu\text{N m)}$	3.354	3.31	3.283	3.261
$T_{cch} \text{ (}\mu\text{N m)}$	2.928	2.782	2.595	2.288
$a_T$	0.87	0.84	0.79	0.7
$b^*$	14.94	14.28	13.29	10.71

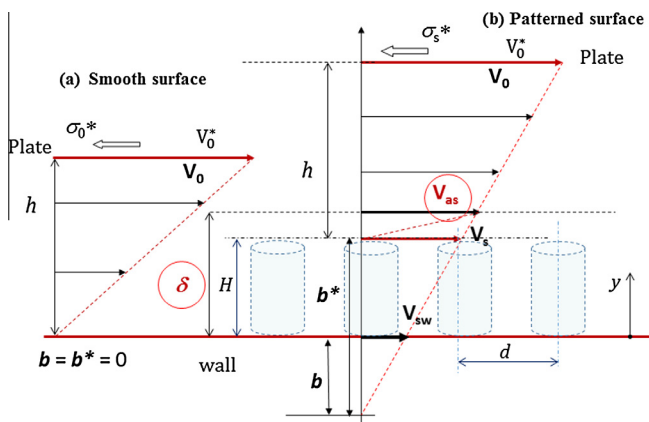


Fig. 19. Simple shear flow in vicinity of smooth and pattern surfaces.

tive at all gaps,  $b^* \ll H$ , see Table 4. Therefore the computed flow regime is characterized by apparent slip on the patterned surface.

Fig. 20 shows the computed *structural parameter*  $b^*$  for the experimental data from Fig. 7. Within the frame of our interpretation, the effective induced slip is present only for the Si-plate pillars pattern ( $H = 9 \mu\text{m}$ , see Fig. 1a), and remarkable only for the Newtonian oil with low viscosity.

This result is consistent with the statement that induced slip at the patterned walls is effective for microgeometries with aspect ratio around one ( $0.5 < H/d < 1.5$ ) for height dimension  $H$  in the range of microns or tens of microns (see Figs. 19 and 1).

In the case of channel pattern the aspect ratio is around one, but the  $H$  value is large, i.e.  $H = 240 \mu\text{m}$ . In this case the microgeometry induces an apparent slip and not an effective slip, since  $b^* \ll H$  for both samples, see Fig. 20.

This conclusion is confirmed by the results from Fig. 21. Here, the results of computations are superimposed for the smooth and patterned channels geometries (end/edge effects, gap error correction, respectively the patterned surface effect) and compared with the measured values (in this representation the assumption that the relative computed correction coefficients have the same values in the range of tested shear rates and viscosities has been considered). The difference between the measurements and the computations are in the range of 10% for the investigated domain.

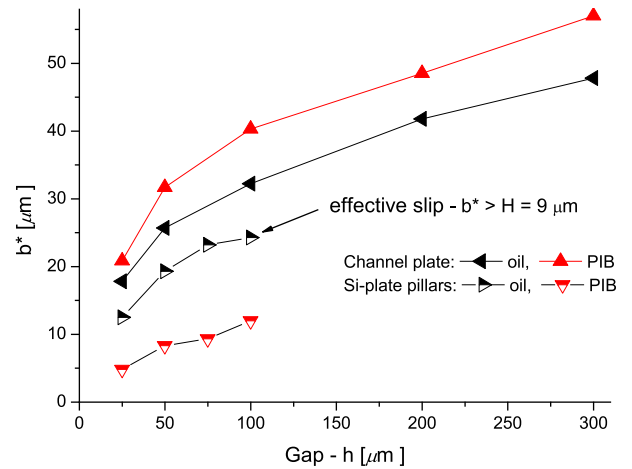


Fig. 20. Variation of parameter  $b^*$  with the gap.

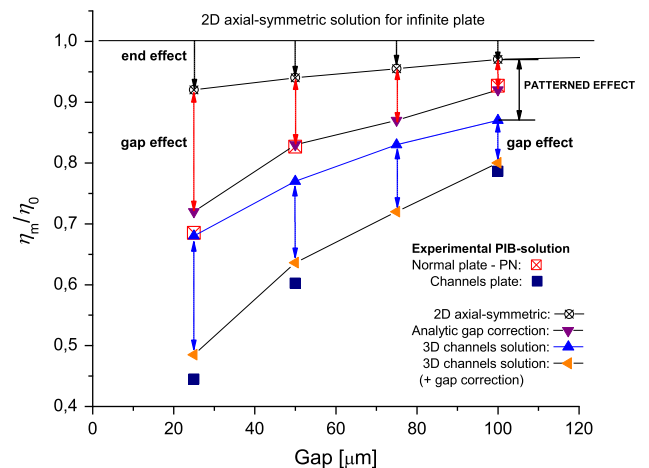


Fig. 21. Computed vs. experimental relative viscosity  $\eta_m/\eta_0$  for  $h \leq 100 \mu\text{m}$  ( $\eta_0$  corresponds at  $h = 200 \mu\text{m}$ ).

The present study demonstrates that hydrophobic effects can be induced to the walls, without violating of the no-slip condition, by changing the local flow spectrum due to the presence of patterned surfaces at the solid boundary. The results confirm that computational rheometry is an useful tool not only to interpret the experimental data and to calculate the errors of the measurements, but also to explore and model flow phenomenon as apparent slip.

In particular, the work was dedicated to the investigation of the influence of patterned surfaces on the measured torque in plate-plate configuration. The correlations of the experimental data with numerical simulations reveal the contribution of the patterned surface on the flow dynamics within the gap and the possibility to make the distinction between the effective and the apparent slip induced by the microgeometry. The paper presented only numerical solutions for pure viscous and Carreau models. Of course, the continuation of the work has to include the effects of elasticity, but this approach is at the moment beyond the computational capabilities available in our group.

This study is considered to be of interest for developing novel techniques in rheometry (using for tests plates with well defined micro-patterned surface) and in microfluidics, where the control of boundary conditions and wall adherence are crucial for many applications.

## Acknowledgements

Corneliu Balan acknowledges the continuous support in his activity offered since 1991 with generosity by Professor Ken Walters FRS.

The authors acknowledge Dr. ing. Catalin Marculescu (IMT Bucharest) and Ph.D. student Amon Klausmann (T.U. Darmstadt) for their assistance in fabrication of the patterned surfaces, and also the financial support from the grants of the Ministry of National Education, Romania, CNCS-UEFISCDI: PN-II-ID-PCE-2012-4-0245 and PN-II-PT-PCCA-2011-3. The work of Nicoleta Octavia Tanase has been funded by the Sectorial Operational Programme Human Resources Development 2007–2013 of the Ministry of European Funds through the Financial Agreement POSDRU/159/1.5/S/132395.

## References

- [1] X. Ding, P. Li, Sz.-C.S. Lin, Z.S. Stratton, N. Nama, F. Guo, D. Slotcavage, X. Mao, J. Shi, F. Costanzo, T.J. Huang, Surface acoustic wave microfluidics, *Lab Chip* 13 (2013) 3626–3649.
- [2] A.D. van der Meer, V.V. Orlova, P. ten Dijke, A. van den Berga, Ch.L. Mummeryd, Three-dimensional co-cultures of human endothelial cells and embryonic stem cell-derived pericytes inside a microfluidic device, *Lab Chip* 13 (2013) 3562–3568.
- [3] A.F. Chrimes, K. Khoshmanesh, P.R. Stoddart, A. Mitchella, K. Kalantar-zadeha, Microfluidics and Raman microscopy: current applications and future challenges, *Chem. Soc. Rev.* 42 (2013) 5880–5906.
- [4] E. Lauga, M.P. Brenner, H.A. Stone, The no-slip boundary condition, in: *Handbook of Experimental Fluid Dynamics*, Springer, Berlin, 2007, pp. 1219–1240.
- [5] T. Sochi, Slip at fluid-solid interface, *Polym. Rev.* 51 (2011) 309–340.
- [6] J.P. Rothstein, Slip on superhydrophobic surfaces, *Annu. Rev. Fluid Mech.* 42 (2010) 89–109.
- [7] D.C. Trethewey, C.D. Meinhart, Apparent fluid slip at hydrophobic micro-channel walls, *Phys. Fluids* 14 (2002) L9–L12.
- [8] S. Heidenreich, P. Ilg, S. Hess, Boundary conditions for fluids with internal orientational degrees of freedom: apparent velocity slip associated with the molecular alignment, *Phys. Rev. E* 75 (2007) 066302.
- [9] N.V. Priezjev, A.A. Darhuber, S.M. Troian, Slip behavior in liquid films on surfaces of patterned wettability: comparison between continuum and molecular dynamics simulations, *Phys. Rev. E* 71 (2005) 041608.
- [10] N.V. Priezjev, S.M. Troian, Influence of periodic wall roughness on the slip behaviour at liquid/solid interfaces: molecular-scale simulations versus continuum predictions, *J. Fluid Mech.* 554 (2006) 25–46.
- [11] O.I. Vinogradova, Slippage of water over hydrophobic surfaces, *Int. J. Miner. Process.* 56 (1999) 31–60.
- [12] S. Granick, Y. Zhu, H.J. Lee, Slippery questions about complex fluids flowing past solids, *Nat. Mater.* 2 (2003) 221–227.
- [13] B.D. Coleman, H. Markovitz, W. Noll, *Viscometric Flows of Non-Newtonian Fluids – Theory and Experiments*, Springer, New York, 1966.
- [14] Y.M. Joshi, A.K. Lele, R.A. Mashelkar, Slipping fluids: a unified transient network model, *J. Non-Newtonian Fluid Mech.* 89 (2000) 303–335.
- [15] R. Buscall, Letter to the editor: wall slip in dispersion rheometry, *J. Rheol.* 54 (2010) 1177–1183.
- [16] A. Yoshimura, R.K. Prudhomme, Wall slip corrections for Couette and parallel disk viscometers, *J. Rheol.* 32 (1988) 53–67.
- [17] H.A. Barnes, A review of the slip (wall depletion) of polymer solutions, emulsions and particle suspensions in viscometers: its cause, character and cure, *J. Non-Newtonian Fluid Mech.* 56 (1995) 221–251.
- [18] K. Walters, *Rheometry*, Chapman and Hall, London, 1976.
- [19] H.A. Barnes, J.F. Hutton, K. Walters, *An Introduction to Rheology*, Elsevier, Amsterdam, 1989.
- [20] M.J. Crochet, A.R. Davies, K. Walters, *Numerical Simulation of Non-Newtonian Flow*, Elsevier, Amsterdam, 1984.
- [21] J. Kramer, J.T. Uhl, R.K. Prudhomme, Measurement of the viscosity of guar gum solutions to 50,000 s<sup>-1</sup> using a parallel plate rheometer, *Polym. Eng. Sci.* 27 (1987) 598–602.
- [22] G.A. Davies, J.R. Stokes, On the gap error in parallel plate rheometry that arises from the presence of air when zeroing the gap, *J. Rheol.* 49 (2005) 919–922.
- [23] O. Kravchuk, J.R. Stokes, Review of algorithms for estimating the gap error correction in narrow gap parallel plate rheology, *J. Rheol.* 57 (2013) 365–375.
- [24] X. Li, H. Tian, J. Shao, Y. Ding, H. Liu, Electrically modulated microtransfer molding for fabrication of micropillar arrays with spatially varying heights, *Langmuir* 29 (2013) 1351–1355.
- [25] Ch. Clasen, G.H. McKinley, Gap-dependent microrheometry of complex liquids, *J. Non-Newtonian Fluid Mech.* 124 (2004) 1–10.
- [26] Ch. Clasen, B.P. Gearing, G.H. McKinley, The flexure-based microgap rheometer (FMR), *J. Rheol.* 50 (2006) 883–905.
- [27] G.A. Davies, J.R. Stokes, Thin film and high shear rheology of multiphase complex fluids, *J. Non-Newtonian Fluid Mech.* 148 (2008) 73–87.
- [28] S.J. Baik, P. Moldenaers, Ch. Clasen, A sliding plate microgap for the simultaneous measurement of shear stress and first normal stress difference, *Rev. Sci. Instrum.* 82 (2011) 035121.
- [29] C. Balan, D. Broboana, E. Ionescu, R. Riedel, Influence of hydrophobic surfaces on the measured rheological properties of complex fluids, in: *The XVth Int. Congress Rheology*, Lisbon, Portugal, August 2012 (pp. 434, book of abstracts).
- [30] Ch. Clasen, H.P. Kavehpour, G.H. McKinley, Bridging tribology and microrheology of thin films, *Appl. Rheol.* 20 (2010) 45049.
- [31] Ch. Clasen, High shear rheometry using hydrodynamic lubrication flows, *J. Rheol.* 57 (2013) 197–221.
- [32] D.J. Acheson, *Elementary Fluid Mechanics*, Clarendon Press, Oxford, 1990.
- [33] F. Durst, *Fluid Mechanics: An Introduction to the Theory of Fluid Flows*, Springer, Berlin, 2008.
- [34] M.Z. Bazant, O.I. Vinogradova, Tensorial hydrodynamic slip, *J. Fluid Mech.* 613 (2008) 125–134.
- [35] K. Kamrin, M.Z. Bazant, H.A. Stone, Effective slip boundary conditions for arbitrary periodic surfaces: the surface mobility tensor, *J. Fluid Mech.* 658 (2010) 409–437.
- [36] E.S. Asmolov, J. Zhou, F. Schmid, O.I. Vinogradova, Effective slip-length tensor for a flow over weakly slipping stripes, *Phys. Rev. E* 88 (2013) 023004.
- [37] C. Schönecker, T. Baier, S. Hardt, Influence of the enclosed fluid on the flow over a microstructured surface in the Cassie state, *J. Fluid Mech.* 740 (2014) 168–195.
- [38] M. Tauviquirrahman, R. Ismail, J. Jamari, D.J. Schipper, A study of surface texturing and boundary slip on improving the load support of lubricated parallel sliding contacts, *Acta Mech.* 224 (2013) 365–381.
- [39] G. Daschiel, M. Perić, J. Jovanović, A. Delgado, The holy grail of microfluidics: sub-laminar drag by layout of periodically embedded microgrooves, *Microfluid. Nanofluid.* <http://dx.doi.org/10.1007/s10404-013-1182-0>.
- [40] D.J. Lee, K.Y. Cho, S. Jang, Y.S. Song, J.R. Youn, Liquid slip on a nanostructured surface, *Langmuir* 28 (2012) 10488–10494.
- [41] Y. Xue, S. Chu, P. Lv, H. Duan, Importance of hierarchical structures in wetting stability on submersed superhydrophobic surfaces, *Langmuir* 28 (2012) 9440–9450.
- [42] C. Lee, C.-J. Kim, Influence of surface hierarchy of superhydrophobic surfaces on liquid slip, *Langmuir* 27 (2011) 4243–4248.